Journal of Colloid and Interface Science 556 (2019) 172–179

Contents lists available at ScienceDirect

Journal of Colloid and Interface Science

journal homepage: www.elsevier.com/locate/jcis

Intrinsically disordered protein as carbon nanotube dispersant: How dynamic interactions lead to excellent colloidal stability

Himanshu Chaudhary [a,*,1], Ricardo M.F. Fernandes [a,c,*,1], Vasantha Gowda [a], Mireille M.A.E. Claessens [b], István Furó [a], Christofer Lendel [a,*]

[a] Department of Chemistry, Division of Applied Physical Chemistry, KTH Royal Institute of Technology, SE-10044 Stockholm, Sweden
[b] MESA + Institute for Nanotechnology and Mira Institute for Biomedical Technology and Technical Medicine, University of Twente, 7500AE Enschede, the Netherlands
[c] Centro de Investigação em Química, Department of Chemistry and Biochemistry, Faculty of Science, University of Porto, Rua do Campo Alegre, s/n, P-4169-007 Porto, Portugal

GRAPHICAL ABSTRACT

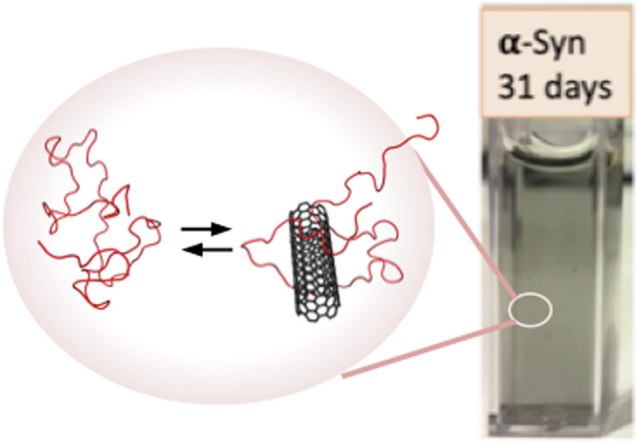

ARTICLE INFO

Article history:
Received 18 June 2019
Revised 12 August 2019
Accepted 13 August 2019
Available online 14 August 2019

Keywords:
α-synuclein
SWNT
NMR

ABSTRACT

The rich pool of protein conformations combined with the dimensions and properties of carbon nanotubes create new possibilities in functional materials and nanomedicine. Here, the intrinsically disordered protein α-synuclein is explored as a dispersant of single-walled carbon nanotubes (SWNTs) in water. We use a range of spectroscopic methods to quantify the amount of dispersed SWNT and to elucidate the binding mode of α-synuclein to SWNT. The dispersion ability of α-synuclein is good even with mild sonication and the obtained dispersion is very stable over time. The whole polypeptide chain is involved in the interaction accompanied by a fraction of the chain changing into a helical structure upon binding. Similar to other dispersants, we observe that only a small fraction (15–20%) of α-synuclein is adsorbed on the SWNT surface with an average residence time below 10 ms.

Abbreviations: 2D, two-dimensional; AFM, atomic force microscopy; BSA, bovine serum albumin; CNT, carbon nanotube; CD, circular dichroism; HSQC, heteronuclear single quantum correlation; IDP, intrinsically disordered protein; NMR, nuclear magnetic resonance; PEO, poly(ethylene oxide); PPO, poly(propylene oxide); SWNT, single-walled carbon nanotube; SSA, specific surface area.

* Corresponding authors at: Department of Chemistry, Division of Applied Physical Chemistry, KTH Royal Institute of Technology, SE-10044 Stockholm, Sweden (C. Lendel).
E-mail addresses: himcha@kth.se (H. Chaudhary), rmff@kth.se (R.M.F. Fernandes), lendel@kth.se (C. Lendel).

[1] These authors contributed equally to the work.

https://doi.org/10.1016/j.jcis.2019.08.050
0021-9797/

Dispersibility
Colloidal stability
Noncovalent functionalization

1. Introduction

The interface between nanotechnology and biotechnology represents an emerging area of research. Through the combination of biomolecules and synthetic nanostructures, such as carbon nanotubes (CNTs), new materials with specific functionalities can be achieved [1,2]. Before integration in materials, exfoliation of pristine CNTs into individual tubes or thin bundles is often required. However, the intrinsic sp^2 carbon structure and strong van der Waals cohesive interactions make the macrobundles of pristine CNTs highly resistant to exfoliation and dispersion in water. Two common strategies to meet this challenge are: (i) covalent binding of hydrophilic functional groups; and (ii) physical adsorption of amphiphilic molecules to the CNTs. The latter option is preferred because the sp^2 hybridization, that confers unique properties to CNTs, is kept intact. Biopolymers such as proteins [3–6], DNA [7–9], and peptides [10,11] are attractive dispersants of CNTs in water as they may add biocompatibility, which is important for biomedical applications [6,12]. Proteins, due to their amphiphilic nature, are assumed to adsorb on the nanotube surface and prevent their re-aggregation through steric and/or electrostatic repulsion between individual CNTs. Adsorption is also essential during the exfoliation stage [13,14]. The binding of proteins to CNTs is governed by their amino acid composition (primary structure) as well as the secondary and tertiary structures [12,15–17]. pH variations may change both the net charge and the conformation of the protein, thereby affect binding and, consequently, CNT dispersibility [3,18].

Up to date, the dispersion of CNTs by a range of proteins with different structures has been studied [11,12,19–23]. However, no reports on the ability of intrinsically disordered proteins (IDPs) to disperse CNTs have been presented. The closest case concerns an engineereed protein domain that is partially disordered [24]. IDPs are proteins that lack a well-defined three-dimensional fold in solution and behave more like random polymer chains [25]. Such proteins could tentatively exploit the full potential of the polypeptide chain as a *block copolymer*. In the present study, we assess the dispersibility of single-walled carbon nanotubes (SWNTs) and the binding mechanism of the IDP α-synuclein, a 14 kDa protein with distinct physicochemical properties in the different regions of the polypeptide chain. The *N*-terminal part is involved in lipid binding and has a propensity to fold into helical structures [26] while the C-terminal part is highly negatively charged at neutral pH. The protein also contains a region with pronounced hydrophobicity, the so-called "NAC" region [27], which plays a central role in the formation of amyloid fibrils. Although α-synuclein is frequently studied, both as a model IDP [28] and because of its association with Parkinson's disease [29] its interaction with CNTs has not been characterized yet.

In order to understand, rationalize and design protein-CNT systems, it is important to assess both structural and dynamic aspects of adsorption. Previously, we have used nuclear magnetic resonance (NMR) diffusometry to study the exchange regime for bovine serum albumin (BSA) and the synthetic block copolymer Pluronic F127 between their respective states in solution and adsorbed at the surface of SWNTs. [4,30] Here, we use the same method supplemented by a number of other spectroscopic and microscopic techniques.

2. Materials and methods

2.1. Materials

CoMoCat single-walled carbon nanotubes of nominal (6,5) chirality and median diameter of 0.78 nm (SG65i, SouthWest NanoTechnologies, dominantly (95%) semiconducting with its largest (41%) single fraction consisting of (6,5) nanotubes with major residual fractions of (8,4), (7,5) and (9,2) nanotubes and, in addition, 28% of nanotubes with unknown chirality) were used as provided by the manufacturer. Pluronic F127 (Sigma-Aldrich product number P2443, ~12.5 kDa), a triblock (PEOx – PPOy – PEOx) polymer with hydrophilic poly(ethylene oxide) (PEO), and hydrophobic poly(propylene oxide) (PPO) blocks with nominal composition of x = 100 and y = 65, heavy water (Sigma-Aldrich, 99.9 atom % D), Tris (Sigma-Aldrich, >99.9% purity) and NaCl (Sigma-Aldrich, >99% purity) were used as received. Expression and purification of α-synuclein was performed as previously described [31]. The protein concentration was estimated by absorbance at 276 nm using a molar extinction coefficient of 5600 M^{-1} cm^{-1}.

2.2. Sample preparation

The SWNT powder (0.29 mg) was dispersed in 900 μL of D_2O. In order to minimize any protein damage due to the strong shear forces created during the ultrasonication process, a combined method of tip- and bath sonication was employed. Before adding any protein, the SWNTs were pre-exfoliated by tip sonication (Qsonica Q500, power density of 1.8 W· mL^{-1} as estimated by calorimetry) [32] during 7 min (2 s on, 10 s off cycle). Even though the nanotubes will re-aggregate in the absence of dispersant, they will not return to the original compact state. Instead, they will form millimeter size aggregates with a mesh-like structure somewhat similar to a loose aggregate recently observed [33]. In the second step, 100 μL of concentrated protein was added (yielding a final protein concentration of 1 mg·mL^{-1}). After 20 min equilibration to enhance the adsorption of protein to the SWNTs, the sample was subjected to the following sonication sequence: 10 min bath sonication (Elma Sonic S10, power density of 3.2×10^{-2} W·mL^{-1}), 1 min tip sonication (2 s on, 10 s off), 15 min bath sonication, 5 min quiescence and 10 min bath sonication; delivering a total energy of approximately 158 J·mL^{-1}. During the whole process the samples were kept in ice/water. To remove any non-dispersed SWNT the sample was centrifuged at 4000 × *g* at 4 °C during 15 min. About 40% of the supernatant was collected and used for further analysis. The amount of SWNT was estimated by UV–vis absorbance (Varian BIO-300 spectrophotometer) at λ = 660 nm with an extinction coefficient ε = 29 mL·mg·cm^{-1} [14]. α-synuclein does not absorb light at this wavelength. A solution of F127 with a final concentration of 1.0 mg mL^{-1} was prepared and added to 0.28 mg of SWNT powder. All procedures were then performed as described for the α-synuclein samples above.

2.3. Colloidal stability assay

The amount of dispersed SWNTs was monitored by UV–vis absorbance (λ = 660 nm) over 30 days of time. The samples were stored at 4 °C for the complete set of experiments.

The α-synuclein/SWNT and F127/SWNT dispersions were diluted 10 times in 10 mM Tris-HCl and 10 mM NaCl buffer (pH 7.4) before the absorbance measurements.

2.4. Atomic force microscopy (AFM)

AFM was performed using a Bruker Dimension Fastscan instrument in tapping mode using Fastscan-A cantilevers (SNL, Bruker, AFM Probes), with a nominal tip radius of 5 nm. The samples for AFM measurements were prepared by depositing approx. 5 μL of SWNTs dispersed by protein on a freshly cleaved mica surface. To remove salt impurities, the sample was rinsed with distilled water. All images were recorded in tapping mode at room temperature under dry conditions. The images were processed and analyzed using NanoScope Analysis v. 1.5 software (Bruker).

2.5. Circular dichroism spectroscopy (CD)

CD measurements were performed using a Chirascan CD Spectrometer (Applied Photophysics) at room temperature in 10 mM Tris-HCl and 10 mM NaCl buffer (pH 7.4) at a protein concentration of 0.1 mg·mL^{-1}. CD spectra were recorded between 190 and 260 nm (with a band width of 1 nm) in a quartz cuvette with 0.1 mm path length. Each spectrum was averaged from 5 accumulative scans. Spectra decomposition was carried out using the BeStSel algorithm [34,35].

2.6. NMR spectroscopy

Two-dimensional (2D) ^{1}H-^{15}N heteronuclear single quantum correlation (HSQC) NMR experiments [36–38], were recorded at 5.0 °C on a 500 MHz Bruker Avance III spectrometer using a sample with 0.1 mM ^{15}N-labelled α-synuclein dissolved in 85% H_2O/15% D_2O. The number of time domain points and acquisition times were 640 points and 210 ms for ^{15}N (F1) and 2048 points and 307 ms for ^{1}H (F2), respectively. A recycle delay of 2.5 s was used. The peak analysis of ^{1}H-^{15}N HSQC spectra were performed using the software PINT [39,40]. Only peaks with fitting quality of 3 or 4 are shown in Fig. 4B.

The transverse relaxation experiments were performed using a 500 MHz Bruker Avance III spectrometer at 5.0 °C. The method is based on a 2D spin echo experiment with the pulse sequence 90° − τ − 180°, using a list of 23 delay times (τ) ranging from 10 ms up to 5 s. The 90° pulse length was 6.5 μs, the recycle delay was set to 3 s and a total of 16 scans were acquired for each spectrum/point. The NMR spin-echo signal decay follows the Bloch equations, expressed as:

$$I = A\exp(-\tau/T_2) \quad (1)$$

where I is the signal intensity from its initial $\tau = 0$ value A, τ is the delay time between the radio frequency pulses, and T_2 is the time constant, called the transverse relaxation time, that characterizes the time required for I to decay down to 1/e (37%). T_2 was obtained by least-square fitting of Eq. (1) to the experimental data.

The ^{1}H NMR diffusion experiments were carried out using a 500 MHz Bruker Advance III spectrometer equipped with a standard-bore magnet and a z-gradient probe DIFF30 (Bruker). The gradient pulses were provided by a Bruker GREAT 60 gradient. The diffusion experiments were performed using the stimulated echo sequence with a 90° pulse length of 6.5 μs, the gradient pulse length set to $\delta = 2$ ms, the gradient stabilization delays to 1 ms, and the diffusion time $\Delta = 10$ ms. The gradient strength g was increased stepwise in 23 steps to a maximum of typically 6.5 T·m^{-1}. All the measurements were carried out at 5.0 °C and the gradient strength was calibrated by measuring the diffusion of ^{1}HDO in D_2O (1.034×10^{-9} m^2·s^{-1} at 5 °C, reference value from literature) [41]. The longitudinal relaxation time, T_1, obtained for protein peaks was 500–600 ms, thus the recycle delay was set to 3 s ($\sim 5T_1$). To allow for small sample volumes ($\sim$100 μL) and provide a homogeneous gradient, 5 mm Shigemi tubes were used. ^{1}HDO peak (T = 5 °C) was calibrated to 5.00 ppm according to the Ref. [42] and additional parameters used were as previously described [4,30,43].

3. Results and discussion

First, pristine SWNT powder added to pure water was presonicated (microTip) to break up the large initial SWNT grains into smaller ones. Addition of concentrated protein solution yielded a mixture with a protein concentration of 1 mg·mL^{-1} that was then subjected to mild sonication (bath). To prevent protein damage, the sonication power was kept at approx. 160 J·mL^{-1}, a much lower value than that used in similar studies [14,32,44–46]. Sonication breakage in synthetic- and biopolymers is often observed at transmitted sonication power/energy densities significantly higher than this [43,47,48]. However, low sonication power can also reduce the reproducibility of the dispersions [32] and we indeed experienced some variation in the final SWNT concentrations (Table 1). This had no apparent effect on the dispersion stability.

The sonicated sample was centrifuged (15 min, 4000 × g), and the upper part of the supernatant (approx. 40%) was collected and the concentration of dispersed SWNT (Table 1) was quantified by measuring the absorbance at λ = 660 nm [49]. Compared to other dispersants, α-synuclein displays a very good dispersion capability. Since the dispersion yield is highly dependent [50] on the preparation protocol and the origin of the SWNTs, a quantitative comparison with other reports is difficult. However, 0.12 mg·mL^{-1} is in level with some of the highest numbers in the literature [51], especially when taking the mild sonication conditions into account. Attempts to disperse SWNTs using the same solution conditions, i.e. Tris-HCl and NaCl in water, but without α-synuclein yielded no measurable SWNT content (data not shown).

For comparison, we applied the same protocol with Pluronic F127 (a widely used dispersant) and found lower amounts of dispersed SWNTs (Table 1). Interestingly, the colloidal stability of the SWNT dispersion in F127 was much lower than for α-synuclein. Over a period of 23 days, the amount of solubilized SWNTs in F127 decreased to approx. 25% of the initial concentration while approx. 90% of the SWNTs were still dispersed with α-synuclein after comparable time (Fig. 1). Similar trends were qualitatively observed in several samples (data not shown).

AFM was used to image the α-synuclein-dispersed SWNTs in a dry state. The SWNTs are visible as fibrillar structures with bead-like objects collected along them that plausibly originate from adsorbed protein (Fig. 2). Cross-sectional profiles at different positions along the SWNTs *between* the "beads" (see example in Fig. 2) provided a height of approx. 0.7 nm that is in good agreement with the median diameter of the SWNTs used (0.78 nm according to the manufacturer). This result proves that α-synuclein exfoliates SWNTs into individual tubes even at mild sonication, a feature that is not common among other dispersants [14,32]. In contrast,

Table 1
The initial SWNT concentration ($c_{SWNT\text{-}init}$), the concentration of SWNTs dispersed in the supernatant ($c_{SWNT\text{-}sup}$) and the yield ($\eta = c_{SWNT\text{-}sup}/c_{SWNT\text{-}init}$) in SWNT dispersions prepared with either α-synuclein or F127. The initial mass concentration of the dispersant was 1 mg mL^{-1} in both cases.

Dispersant	$c_{SWNT\text{-}init}$/mg mL^{-1}	$c_{SWNT\text{-}sup}$/mg mL^{-1}	η
α-synuclein	0.29	0.12 ± 0.085	0.41
F127	0.28	0.048 ± 0.02	0.17

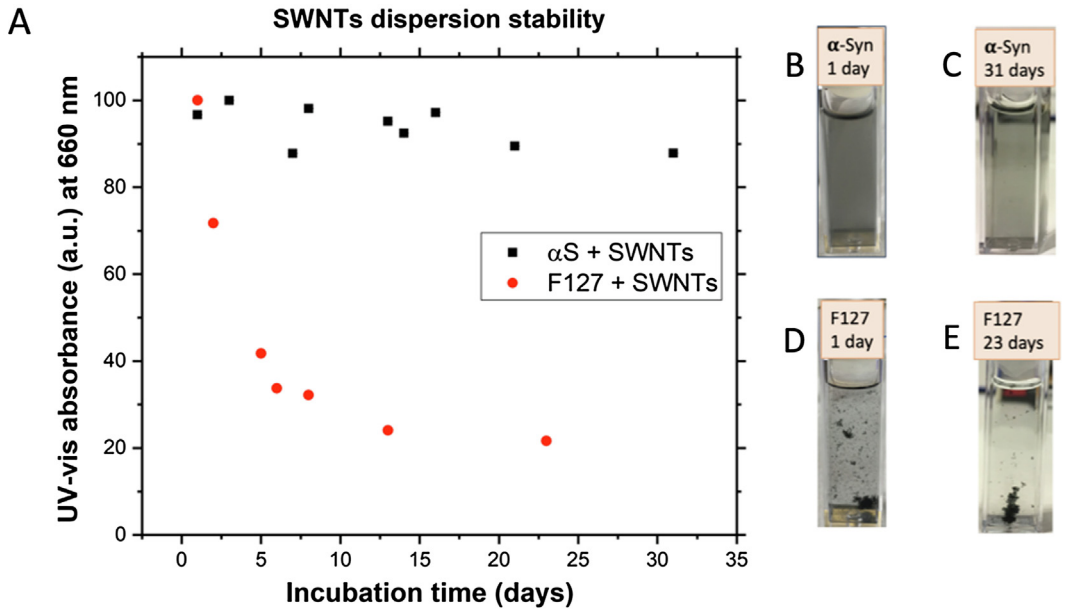

Fig. 1. SWNT dispersion stability assay. (A) Normalized amounts of dispersed SWNTs in the supernatant at set times after preparation, as estimated by UV–Vis absorbance at 660 nm. (B) and (C) show an α-synuclein-based SWNT dispersion at day 1 and day 31, respectively, while (D) and (E) show an F127-based SWNTs dispersion at day 1 and day 23, respectively.

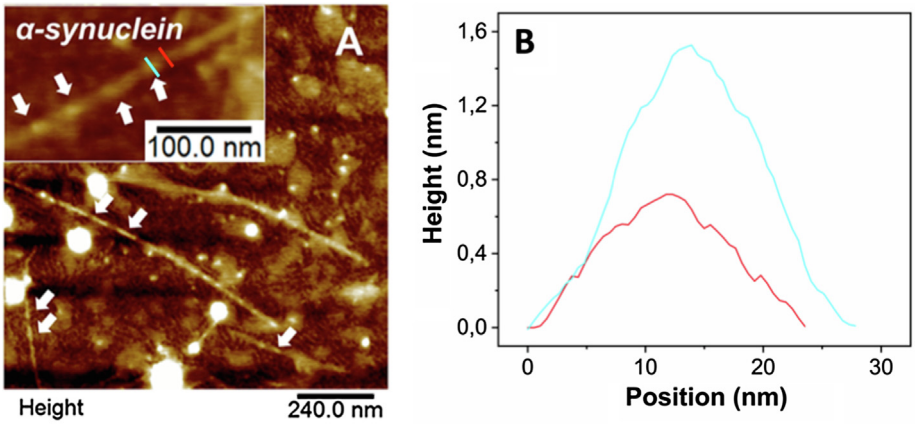

Fig. 2. (A) Single SWNTs could be visualized using AFM. White arrows point to objects that are interpreted as proteins adsorbed onto SWNTs. The inset highlights the bead-like objects on SWNTs. (B) Representative cross-sectional profiles of the SWNTs at positions that coincide (light blue) or do not coincide (red) with beads. Lines with matching color in A indicate the actual measuring positions. (For interpretation of the references to color in this figure legend, the reader is referred to the web version of this article.)

cross-sectional profiles coinciding with the "beads" provided significantly higher profiles (approx. 1.5 nm) that we interpret as one or a few bound α-synuclein molecules adsorbed to the SWNT. Although the hydrodynamic radius of α-synuclein in solution is around 2.7 nm [52], the bound form could be more compact, in particular in the dry state examined by AFM. A recent AFM study of monomeric α-synuclein in solution suggest an apparent height of 1.0–1.5 nm for extended conformations of the protein [53].

By comparing the ^{1}H NMR intensities (Fig. S1 in Supplementary material) of protein peaks in neat protein solutions and in the prepared dispersions, we estimated the remaining concentration of α-synuclein in the supernatant to $c_{\alpha\text{-syn-sup}} \approx 0.8$ mg mL^{-1}, i.e. 20% less than the initial concentration. The signal loss can be assumed to originate from protein depletion by adsorption to the precipitated portion of SWNTs, as observed for other dispersants [54]. In order to quantify the fraction of adsorbed α-synuclein on the *dispersed* SWNTs we rely on ^{1}H NMR diffusometry. This approach has previously been used to characterize molecular aspects of interactions between SWNT and various dispersing agents, such as the surface coverage by and average residence time of the dispersant adsorbed on SWNT [4,14,30,55,56]. The diffusional decays recorded for several ^{1}H spectral sections of α-synuclein in a neat protein solution and in an SWNT dispersion prepared by α-synuclein are shown in Fig. 3 (see also Fig. S2 in Supplementary material). The decays seem to be single-exponential down to a few percent of the initial intensity which indicates that, on the time scale set by the selected diffusion time $\Delta = 10$ ms, the α-synuclein molecular displacement is characterized by a single self-diffusion coefficient D_{obs}. The SWNT-surface-bound and free-in-bulk states of α-synuclein must attain different diffusion coefficients, D_{bound} and D_{free}, respectively, as explicitly shown to be the case for other dispersants [43]. The presence of a single experimental D_{obs} indicates that, under current conditions, the experiment detects the population average expressed as:

$$D_{obs} = (1 - p_{bound})D_{free} + p_{bound} \times D_{bound} \quad (2)$$

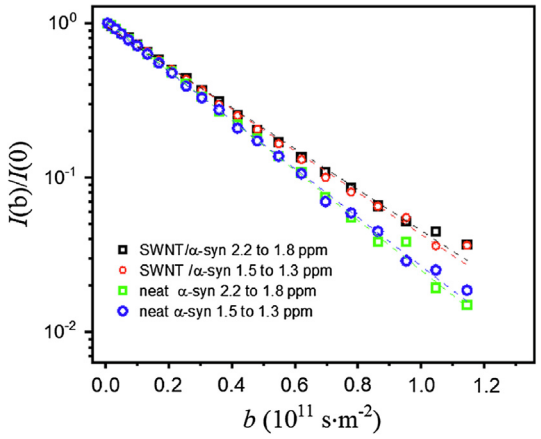

Fig. 3. ^{1}H NMR diffusional decays of defined spectral integrals within the α-synuclein spectrum as a function of the Stejskal-Tanner [69] factor $b = (\gamma g \delta)^2 (\Delta - \delta/3)$ where γ is the magnetogyric ratio of ^{1}H and the other experimental parameters are defined in the Supplementary material. Data for neat solutions (green, blue) and SWNT/α-synuclein dispersions (black, red) are shown. (For interpretation of the references to color in this figure legend, the reader is referred to the web version of this article.)

where p_{bound} corresponds to populations of the bound state. Instrumental limitations prohibit experiments with $\Delta < 10$ ms, and therefore we cannot explore the exchange process [43] in greater detail.

With D_{free} obtained from a neat protein solution (Table 2) and assuming $D_{free} \gg D_{bound}$ [4,43], p_{bound} can be estimated as:

$$p_{bound} \approx 1 - \frac{D_{obs}}{D_{free}} \quad (3)$$

Table 2
Self-diffusion coefficients obtained from the fitting in different regions of the ^{1}H spectrum of neat α-synuclein and SWNT dispersion. The diffusional signal decays for integration regions are shown in Fig. 3 and Supplementary material Fig. S2. The estimated precision of the extracted average diffusion coefficients is in the order of ±1.5% (while accuracy is in the order of ±2.5% as affected by gradient calibration) [70]. The extracted p_{bound} parameter is insensitive, see Eq. (3), to calibration errors.

Integration region	3.09–2.8 ppm	2.2–1.8 ppm	1.5–1.3 ppm	1.0–1.3 ppm
Self-diffusion coef.	$D/10^{-11}$ $m^2\ s^{-1}$	$D/10^{-11}$ $m^2\ s^{-1}$	$D/10^{-11}$ $m^2\ s^{-1}$	$D/10^{-11}$ $m^2\ s^{-1}$
D_{free} (Neat α-syn)	4.11	3.72	3.62	4.11
D_{obs} (SWNT/α-syn)	3.23	3.05	3.12	3.52
p_{bound}	0.21	0.18	0.14	0.14

The results are shown in Table 2. The self-diffusion coefficients derived from different chemical shift ranges within the protein spectrum differ from each other more than would be expected by random experimental error typical for diffusion experiments. Since the relative variation is similar in neat samples and the SWNT dispersions, this seems to be caused by some minor non-protein impurity with a diffusion coefficient different from that of α-synuclein. Yet, the data consistently yield p_{bound} in the order of 15–20%. This points to the same limitation by microscopic kinetics to the dispersion process that was observed for other systems [14].

The fractions of SWNT-bound dispersants, which have not been quantified in many studies, were previously determined to be approx. 4% in SWNT/BSA [4] and 4–6% SWNT/F127 [14,30]. Compared to those systems, the bound fraction of the α-synuclein dispersant is relatively high, which could point to a stronger binding

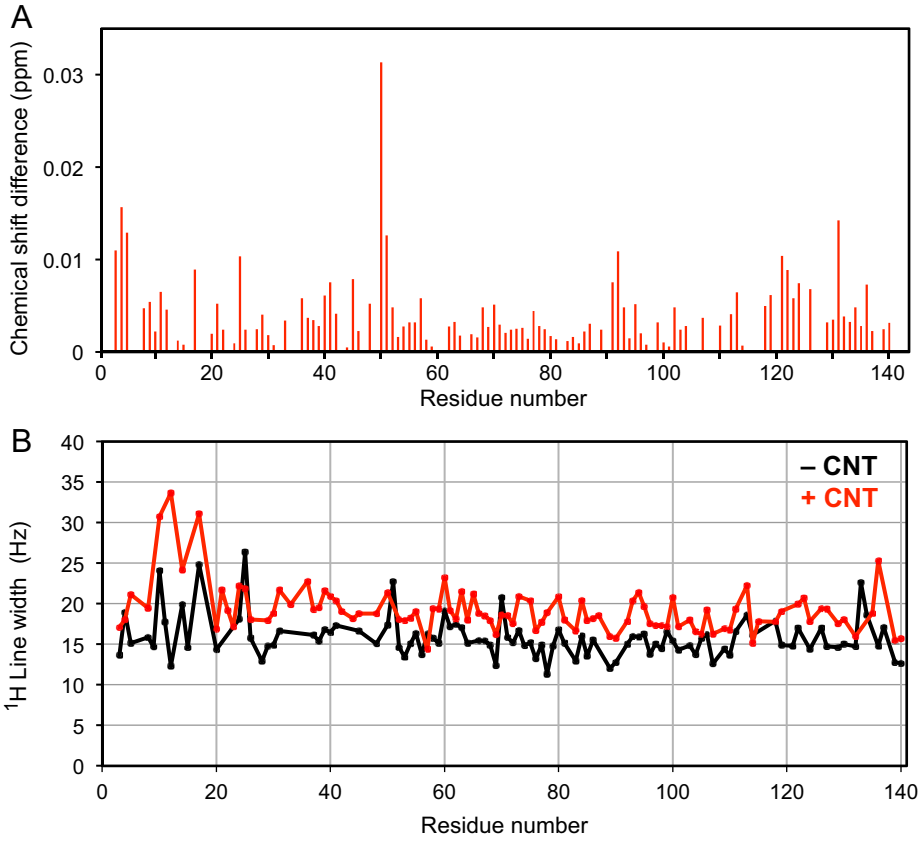

Fig. 4. Changes in the ^{1}H-^{15}N HSQC spectrum of α-synuclein upon binding to SWNTs. (A) Weighted $^1H^{15}N$ chemical shift changes $[\Delta\delta(^1H)^2 + (0.2 \cdot \Delta\delta(^{15}N))^2]^{1/2}$. (B) ^{1}H linewidths for residues with good quality lineshape fitting.

to the SWNT. Yet, in contrast to F127, the residence time of α-synuclein on the SWNT surface is one order of magnitude shorter, which indicates weaker interactions (under the assumption of a first-order process for desorption) [57].

Combining the $c_{\alpha\text{-syn-sup}}$ with p_{bound} and the $c_{\text{SWNT-sup}}$, the surface coverage can be estimated as $p_{\text{bound}} \times c_{\alpha\text{-syn-sup}}/c_{\text{SWNT-sup}}$, yielding 0.64 mg (α-synuclein)/mg (SWNT). This value is slightly above the approx. 0.5 mg (dispersant)/mg (SWNT) obtained in previous work using F127 as dispersant [30]. One possible explanation for this observation is a higher degree of exfoliation by α-synuclein, leading to more individual nanotubes (as compared to a higher proportion of thin bundles obtained by F127). Indeed, the AFM analysis of the SWNT/α-synuclein dispersion, together with the lack of SWNT aggregation during the colloidal stability assay, indicates that the degree of exfoliation of nanotubes by α-synuclein is quite high. Assuming a theoretical specific surface area (SSA) [58] of the SWNT = 1315 $m^2\ g^{-1}$ (corresponding to full exfoliation) being valid here, the area per adsorbed α-synuclein molecule (A_s) on the SWNT surface is $A_s = 47\ nm^2$. With due caution, mainly to different experimental conditions and assumptions (e.g. dispersant and SWNT concentrations, assumed SWNT SSA, etc.), we observe that the obtained $A_s = 47\ nm^2$ is line with reported values for BSA [4], F127 [59] and blood proteins [60].

Besides diffusion NMR experiments, 2D heteronuclear ^1H-^{15}N correlation (HSQC) spectroscopy is a frequently used NMR method to probe molecular interactions of proteins, including binding of α-synuclein to various ligands [61–65]. In an attempt to reveal structural alterations in α-synuclein upon association to the SWNT surface, ^1H-^{15}N HSQC spectra were recorded for α-synuclein alone and in the samples with SWNTs. We observe only minor changes in the chemical shifts of the peaks (Fig. 4A) with the largest changes for the histidine in position 50, which is notoriously sensitive to changes in the surrounding. This also confirms that sonication did not cause any damage to the protein. In addition, the apparent ^1H linewidths become larger for all residues (20 ± 5 Hz in the dispersion compared to 17 ± 5 Hz in pure α-synuclein solution) (Fig. 4B). This general increase is, probably to a large part, a consequence of the presence of paramagnetic impurities in the SWNTs (e.g. Co and Mo as catalyst for preparation). Indeed, the homogeneous line width (as detected by spin echo experiments, see materials and methods) for the ^1HDO peak of water increases from approx. 1 Hz to approx. 10 Hz upon the dispersion of SWNTs. Beside the general increase, the line width increases more for some residues in the N-terminal region. Notably, the same region displays the largest linewidths also in the free protein, which makes it difficult to speculate about the role of this region in the binding process.

CD spectra were measured in the absence and presence of SWNTs (Fig. 5A) to assess how SWNT-binding affects the secondary structure of α-synuclein. The spectrum of the free protein indicates mostly random coil structures, as previously reported [26,65–67]. The difference spectrum (Fig. 5B), representative of the 15–20% of the protein molecules in the bound state, is clearly different from that in the free state and is similar to spectra expected for α-helical proteins. Spectral decomposition [34,35] confirms that the helical component exhibits the largest relative increase in structural content upon binding (see Table S1 in Supplementary material). Indeed, α-synuclein is known to fold into helical structures upon binding to lipid membranes and membrane mimics [26,66] and similar structural transformations seem to occur also when binding to hydrophobic SWNTs. However, the uniform chemical shift changes (Fig. 4A) indicate that the transition is *not* located at specific regions of the protein chain. Helical secondary structures have previously been observed to constitute the CNT-binding segment of lysozyme by molecular dynamics simulations

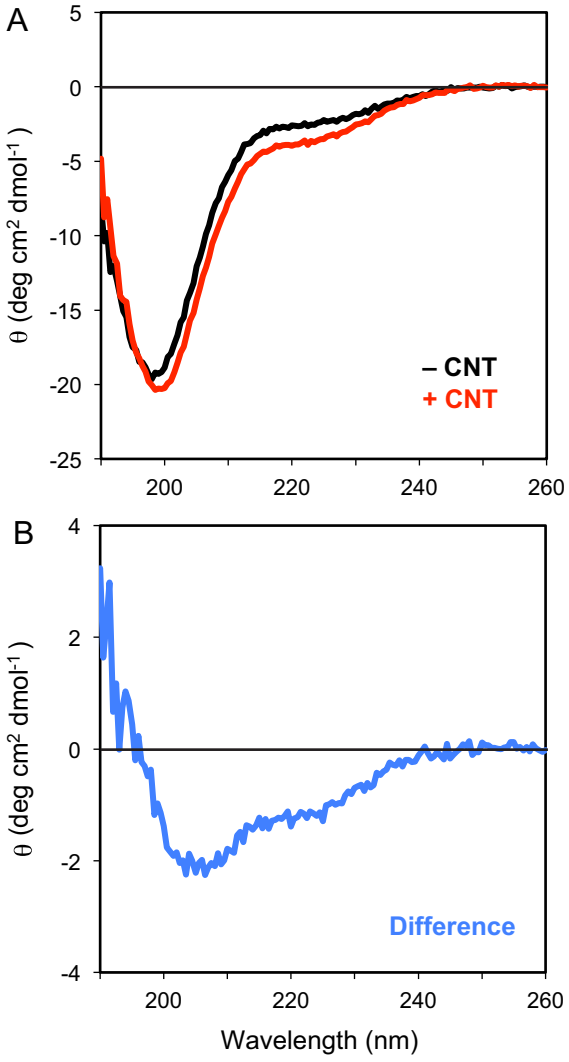

Fig. 5. (A) CD spectra recorded for α-synuclein with (+) and without (−) SWNTs. (B) The difference spectrum of the two spectra in panel A.

[68]. Simulations of the interactions of an IDP are, however, very challenging because of the lack of a defined native structure.

4. Conclusions

Our results demonstrate that IDPs, exemplified in this study by α-synuclein, can be highly efficient dispersing agents for SWNTs, yielding very stable dispersions with a high degree of SWNT exfoliation. Full exfoliation was indeed observed by AFM. NMR diffusometry shows that 15–20% of the protein is adsorbed on the SWNT, which is *higher* than that in previously studied dispersants. The residence time on the surface is, however, *shorter* (below 10 ms) than for many other dispersants. Although CD spectroscopy indicates the formation of helical secondary structures in the protein upon binding, HSQC NMR did not reveal any specific regions of the α-synuclein that are responsible for the interaction with the SWNTs. Hence, the binding does not rely on the block copolymer-like structure of the amino acid sequence of α-synuclein. We hypothesize that, while the instantaneous binding fraction of the chain matches its conformation so that the binding to SWNTs is strong, the major non-binding part of the α-synuclein chain remains disordered and freely fluctuating (as do other

random polymers in a solvent). This fluctuating part may occasionally destabilize the binding competent conformation and thereby the protein can detach. The binding fraction can be anywhere in the chain and thereby we observe no specific effects along the sequence. This scenario is consistent with the experimental findings we present. Taken together, our study suggests a potential for intrinsically disordered proteins to enhance the solubility of nanomaterials in general. The possibility to disconnect the interaction from specific tertiary structures of the protein facilitates the use of biotechnological methods to redesign and optimize protein-based dispersants.

Acknowledgments

We thank K.A. van Leijenhorst Groener for expression and purification of α-synuclein. This work has been supported by the Swedish Research Council VR. RF thanks to CIQUP for financial support through FEDER, Portugal, COMPETE, Portugal, and Fundação para a Ciência e Tecnologia (FCT), Portugal through grants UID/QUI/00081/2013, POCI-01-0145-FEDER-006980, and NORTE- 01-0145-FEDER-000028.

Appendix A. Supplementary material

Supplementary data to this article can be found online at https://doi.org/10.1016/j.jcis.2019.08.050.

References

[1] C. Li, R. Mezzenga, The interplay between carbon nanomaterials and amyloid fibrils in bio-nanotechnology, Nanoscale 5 (2013) 6207–6218.
[2] E. Gazit, Plenty of Room for Biology at the Bottom: An Introduction to Bionanotechnology, second ed., Imperial College Press, London, 2013.
[3] E. Edri, O. Regev, "Shaken, Not Stable": dispersion mechanism and dynamics of protein-dispersed nanotubes studied via spectroscopy, Langmuir 25 (2009) 10459–10465.
[4] A.E. Frise, E. Edri, I. Furó, O. Regev, Protein dispersant binding on nanotubes studied by NMR self-diffusion and cryo-TEM techniques, J. Phys. Chem. Lett. 1 (2010) 1414–1419.
[5] S. Marchesan, M. Prato, Under the lens: carbon nanotube and protein interaction at the nanoscale, Chem. Commun. 51 (2015) 4347–4359.
[6] F. Bomboi, A. Bonincontro, C. La Mesa, F. Tardani, Interactions between single-walled carbon nanotubes and lysozyme, J. Colloid Interface Sci. 355 (2011) 342–347.
[7] M. Zheng, A. Jagota, E.D. Semke, B.A. Diner, R.S. McLean, S.R. Lustig, R.E. Richardson, N.G. Tassi, DNA-assisted dispersion and separation of carbon nanotubes, Nat. Mater. 2 (2003) 338–342.
[8] D. Roxbury, X. Tu, M. Zheng, A. Jagota, Recognition ability of DNA for carbon nanotubes correlates with their binding affinity, Langmuir 27 (2011) 8282–8293.
[9] G. Ao, J.K. Streit, J.A. Fagan, M. Zheng, Differentiating left- and right-handed carbon nanotubes by DNA, J. Am. Chem. Soc. 138 (2016) 16677–16685.
[10] N.M.B. Cogan, C.J. Bowerman, L.J. Nogaj, B.L. Nilsson, T.D. Krauss, Selective suspension of single-walled carbon nanotubes using β-sheet polypeptides, J. Phys. Chem. C 118 (2014) 5935–5944.
[11] Z. Li, T. Kameda, T. Isoshima, E. Kobatake, T. Tanaka, Y. Ito, M. Kawamoto, Solubilization of single-walled carbon nanotubes using a peptide aptamer in water below the critical micelle concentration, Langmuir 31 (2015) 3482–3488.
[12] M. Calvaresi, F. Zerbetto, The devil and holy water: protein and carbon nanotube hybrids, Acc. Chem. Res. 46 (2013) 2454–2463.
[13] M.S. Strano, V.C. Moore, M.K. Miller, The role of surfactant adsorption during ultrasonication in the dispersion of single-walled carbon nanotubes, J. Nanosci. Nanotechnol. 3 (2003) 81–86.
[14] J. Dai, R.M.F. Fernandes, O. Regev, E.F. Marques, I. Furó, Dispersing carbon nanotubes in water with amphiphiles: dispersant adsorption, kinetics, and bundle size distribution as defining factors, J. Phys. Chem. C 122 (2018) 24386–24393.
[15] A. Antonucci, J. Kupis-Rozmysłowicz, A.A. Boghossian, Noncovalent protein and peptide functionalization of single-walled carbon nanotubes for biodelivery and optical sensing applications, ACS Appl. Mater. Interfaces 9 (2017) 11321–11331.
[16] Z. He, J. Zhou, Probing carbon nanotube–amino acid interactions in aqueous solution with molecular dynamics simulations, Carbon 78 (2014) 500–509.
[17] K. Matsuura, T. Saito, T. Okazaki, S. Ohshima, M. Yumura, S. Iijima, Selectivity of water-soluble proteins in single-walled carbon nanotube dispersions, Chem. Phys. Lett. 429 (2006) 497–502.
[18] D. Nepal, K.E. Geckeler, PH-sensitive dispersion and debundling of single-walled carbon nanotubes: lysozyme as a tool, Small 2 (2006) 406–412.
[19] S.F. Oliveira, G. Bisker, N.A. Bakh, S.L. Gibbs, M.P. Landry, M.S. Strano, Protein functionalized carbon nanomaterials for biomedical applications, Carbon 95 (2015) 767–779.
[20] E. Edri, O. Regev, PH Effects on BSA-dispersed carbon nanotubes studied by spectroscopy-enhanced composition evaluation techniques, Anal. Chem. 80 (2008) 4049–4054.
[21] D. Nepal, K.E. Geckeler, Proteins and carbon nanotubes: close encounter in water, Small 3 (2007) 1259–1265.
[22] A.W.N. Sloan, A.L.R. Santana-Pereira, J. Goswami, M.R. Liles, V.A. Davis, Single-walled carbon nanotube dispersion in tryptic soy broth, ACS Macro Lett. 6 (2017) 1228–1231.
[23] D.W. Horn, K. Tracy, C.J. Easley, V.A. Davis, Lysozyme dispersed single-walled carbon nanotubes: interaction and activity, J. Phys. Chem. C 116 (2012) 10341–10348.
[24] P.D. Boyer, S. Ganesh, Z. Qin, B.D. Holt, M.J. Buehler, M.F. Islam, K.N. Dahl, Delivering single-walled carbon nanotubes to the nucleus using engineered nuclear protein domains, ACS Appl. Mater. Interfaces 8 (2016) 3524–3534.
[25] C.J. Oldfield, A.K. Dunker, Intrinsically disordered proteins and intrinsically disordered protein regions, Annu. Rev. Biochem. 83 (2014) 553–584.
[26] D. Eliezer, E. Kutluay, R. Bussell, G. Browne, Conformational properties of α-synuclein in its free and lipid-associated states, J. Mol. Biol. 307 (2001) 1061–1073.
[27] E.A. Waxman, J.R. Mazzulli, B.I. Giasson, Characterization of hydrophobic residue requirements for α-synuclein fibrillization, Biochemistry 48 (2009) 9427–9436.
[28] C. Lendel, P. Damberg, 3D J-resolved NMR spectroscopy for unstructured polypeptides: fast measurement of $^{3}J_{HNH\alpha}$ coupling constants with outstanding spectral resolution, J. Biomol. NMR 44 (2009) 35–42.
[29] L. Stefanis, α-synuclein in Parkinson's disease, Cold Spring Harb. Perspect. Med. 2 (2012) a009399.
[30] R.M.F. Fernandes, M. Buzaglo, O. Regev, E.F. Marques, I. Furó, Surface coverage and competitive adsorption on carbon nanotubes, J. Phys. Chem. C 119 (2015) 22190–22197.
[31] H. Chaudhary, V. Subramaniam, M.M.A.E. Claessens, Direct visualization of model membrane remodeling by α-synuclein fibrillization, Chem. Phys. Chem. 18 (2017) 1620–1626.
[32] R.M.F. Fernandes, B. Abreu, B. Claro, M. Buzaglo, O. Regev, I. Furó, E.F. Marques, Dispersing carbon nanotubes with ionic surfactants under controlled conditions: comparisons and insight, Langmuir 31 (2015) 10955–10965.
[33] R.M.F. Fernandes, M. Buzaglo, O. Regev, I. Furó, E.F. Marques, Mechanical agitation induces counterintuitive aggregation of pre-dispersed carbon nanotubes, J. Colloid Interface Sci. 493 (2017) 398–404.
[34] A. Micsonai, F. Wien, L. Kernya, Y.-H. Lee, Y. Goto, M. Réfrégiers, J. Kardos, Accurate secondary structure prediction and fold recognition for circular dichroism spectroscopy, Proc. Natl. Acad. Sci. USA 112 (2015) E3095–E3103.
[35] A. Micsonai, F. Wien, É. Bulyáki, J. Kun, É. Moussong, Y.-H. Lee, Y. Goto, M. Réfrégiers, J. Kardos, BeStSel: a web server for accurate protein secondary structure prediction and fold recognition from the circular dichroism spectra, Nucl. Acids Res. 46 (2018) W315–W322.
[36] A.G. Palmer, J. Cavanagh, P.E. Wright, M. Rance, Sensitivity improvement in proton-detected two-dimensional heteronuclear correlation NMR spectroscopy, J. Magn. Reson 93 (1991) 151–170.
[37] L. Kay, P. Keifer, T. Saarinen, Pure absorption gradient enhanced heteronuclear single quantum correlation spectroscopy with improved sensitivity, J. Am. Chem. Soc. 114 (1992) 10663–11065.
[38] J.J. Schleucher, M. Schleucher, M. Schwendinger, P. Sattler, O. Schedletzky Schmidt, S.J. Glaser, O.W. Sørensen, C. Griesinger, A general enhancement scheme in heteronuclear multidimensional NMR employing pulsed field gradients, J. Biomol. NMR 4 (1994) 301–306.
[39] A. Ahlner, M. Carlsson, B.-H. Jonsson, P. Lundström, PINT: a software for integration of peak volumes and extraction of relaxation rates, J. Biomol. NMR 56 (2013) 191–202.
[40] M. Niklasson, R. Otten, A. Ahlner, C. Andresen, J. Schlagnitweit, K. Petzold, P. Lundström, Comprehensive analysis of NMR data using advanced line shape fitting, J. Biomol. NMR 69 (2017) 93–99.
[41] R. Mills, Self-diffusion in normal and heavy water in the range 1–45. Deg, J. Phys. Chem. 77 (1973) 685–688.
[42] H.E. Gottlieb, V. Kotlyar, A. Nudelman, NMR chemical shifts of common laboratory solvents as trace impurities, J. Org. Chem. 62 (1997) 7512–7515.
[43] R.M.F. Fernandes, M. Buzaglo, M. Shtein, I. Pri Bar, O. Regev, E.F. Marques, I. Furó, Lateral diffusion of dispersing molecules on nanotubes as probed by NMR, J. Phys. Chem. C 118 (2014) 582–589.
[44] A.J. Blanch, C.E. Lenehan, J.S. Quinton, Parametric analysis of sonication and centrifugation variables for dispersion of single walled carbon nanotubes in aqueous solutions of sodium dodecylbenzene sulfonate, Carbon 49 (2011) 5213–5228.
[45] R. Fuge, M. Liebscher, C. Schröfl, S. Oswald, A. Leonhardt, B. Büchner, V. Mechtcherine, Fragmentation characteristics of undoped and nitrogen-doped multiwalled carbon nanotubes in aqueous dispersion in dependence on the ultrasonication parameters, Diam. Relat. Mater. 66 (2016) 126–134.
[46] K.G. Dassios, P. Alafogianni, S.K. Antiohos, C. Leptokaridis, N.-M. Barkoula, T.E. Matikas, Optimization of sonication parameters for homogeneous surfactant-assisted dispersion of multiwalled carbon nanotubes in aqueous solutions, J. Phys. Chem. C 119 (2015) 7506–7516.

[47] S. Koda, Ultrasonic degradation of water-soluble polymers, Polymer 35 (1994) 30–33.
[48] M.L. Tsaih, R.H. Chen, Effect of degree of deacetylation of chitosan on the kinetics of ultrasonic degradation of chitosan, J. Appl. Polym. Sci. 90 (2003) 3526–3531.
[49] M. Shtein, I. Pri-bar, O. Regev, A simple solution for the determination of pristine carbon nanotube concentration, Analyst 138 (2013) 1490–1496.
[50] W.H. Duan, Q. Wang, F. Collins, Dispersion of carbon nanotubes with SDS surfactants: a study from a binding energy perspective, Chem. Sci. 2 (2011) 1407.
[51] K. Kurppa, H. Jiang, G.R. Szilvay, A.G. Nasibulin, E.I. Kauppinen, M.B. Linder, Controlled hybrid nanostructures through protein-mediated noncovalent functionalization of carbon nanotubes, Angew. Chem. Int. Ed. Engl. 46 (2007) 6446–6449.
[52] A.S. Morar, A. Olteanu, G.B. Young, G.J. Pielak, Solvent-induced collapse of α-synuclein and acid-denatured cytochrome C, Protein Sci. 10 (2001) 2195–2199.
[53] Y. Zhang, M. Hashemi, Z. Lv, B. Williams, K.I. Popov, N.V. Dokholyan, Y.L. Lyubchenko, High-speed atomic force microscopy reveals structural dynamics of α-synuclein monomers and dimers, J. Chem. Phys. 148 (2018) 123322.
[54] R.M.F. Fernandes, J. Dai, O. Regev, E.F. Marques, I. Furó, Block copolymers as dispersants for single-walled carbon nanotubes: modes of surface attachment and role of block polydispersity, Langmuir 34 (2018) 13672–13679.
[55] T.A. Shastry, A.J. Morris-Cohen, E.A. Weiss, M.C. Hersam, Probing carbon nanotube-surfactant interactions with two-dimensional DOSY NMR, J. Am. Chem. Soc. 135 (2013) 6750–6753.
[56] H. Kato, A. Nakamura, M. Horie, Behavior of surfactants in aqueous dispersions of single-walled carbon nanotubes, RSC Adv. 4 (2014) 2129–2136.
[57] J.F. Douglas, H.E. Johnson, S. Granick, A simple kinetic model of polymer adsorption and desorption, Science 262 (1993) 2010–2012.
[58] A. Peigney, C. Laurent, E. Flahaut, R.R. Bacsa, A. Rousset, Specific surface area of carbon nanotubes and bundles of carbon nanotubes, Carbon 39 (2001) 507–514.
[59] A.E. Frise, G. Pagès, M. Shtein, I. Pri Bar, O. Regev, I. Furó, Polymer binding to carbon nanotubes in aqueous dispersions: residence time on the nanotube surface as obtained by NMR diffusometry, J. Phys. Chem. B 116 (2012) 2635–2642.
[60] C. Ge, J. Du, L. Zhao, L. Wang, Y. Liu, D. Li, Y. Yang, R. Zhou, Y. Zhao, Z. Chai, et al., Binding of blood proteins to carbon nanotubes reduces cytotoxicity, Proc. Natl. Acad. Sci. USA 108 (2011) 16968–16973.
[61] C.O. Fernández, W. Hoyer, M. Zweckstetter, E.A. Jares-Erijman, V. Subramaniam, C. Griesinger, T.M. Jovin, NMR of α-synuclein-polyamine complexes elucidates the mechanism and kinetics of induced aggregation, Eur. Mol. Biol. Org. J. 23 (2004) 2039–2046.
[62] F.E. Herrera, A. Chesi, K.E. Paleologou, A. Schmid, A. Munoz, M. Vendruscolo, S. Gustincich, H.A. Lashuel, P. Carloni, Inhibition of α-synuclein fibrillization by dopamine is mediated by interactions with five C-terminal residues and with E83 in the NAC region, PLoS One 3 (2008) e3394.
[63] W.S. Woods, J.M. Boettcher, D.H. Zhou, K.D. Kloepper, K.L. Hartman, D.T. Ladror, Z. Qi, C.M. Rienstra, J.M. George, Conformation-specific binding of α-synuclein to novel protein partners detected by phage display and NMR spectroscopy, J. Biol. Chem. 282 (2007) 34555–34567.
[64] Z. Zhang, C. Dai, J. Bai, G. Xu, M. Liu, C. Li, Ca^{2+} modulating α-synuclein membrane transient interactions revealed by solution NMR spectroscopy, Biochim. Biophys. Acta 1838 (2014) 853–858.
[65] C. Lendel, C.W. Bertoncini, N. Cremades, C.A. Waudby, M. Vendruscolo, C.M. Dobson, D. Schenk, J. Christodoulou, G. Toth, On the mechanism of nonspecific inhibitors of protein aggregation: dissecting the interactions of α-synuclein with Congo red and lacmoid, Biochem. 48 (2009) 8322–8334.
[66] W.S. Davidson, A. Jonas, D.F. Clayton, J.M. George, Stabilization of α-synuclein secondary structure upon binding to synthetic membranes, J. Biol. Chem. 273 (1998) 9443–9449.
[67] Y. Cai, C. Lendel, L. Österlund, A. Kasrayan, L. Lannfelt, M. Ingelsson, F. Nikolajeff, M. Karlsson, J. Bergström, Changes in secondary structure of α-synuclein during oligomerization induced by reactive aldehydes, Biochem. Biophys. Res. Commun. 464 (2015) 336–341.
[68] M. Calvaresi, S. Hoefinger, F. Zerbetto, Probing the structure of lysozyme-carbon-nanotube hybrids with molecular dynamics, Chem. Eur. J. 18 (2012) 4308–4313.
[69] E.O. Stejskal, J.E. Tanner, Spin diffusion measurements: spin echoes in the presence of a time-dependent field gradient, J. Chem. Phys. 42 (1965) 288–292.
[70] W.S. Price, NMR Studies of Translational Motion: Principles and Applications, Cambridge University Press, Cambridge, 2009.